coatings

MDPI

Article

Assessment of Super-Hydrophobic Textured Coatings on AA6082 Aluminum Alloy

Luigi Calabrese [1,*], Amani Khaskhoussi [1,2], Salvatore Patane [3] and Edoardo Proverbio [1]

1 Department of Engineering, University of Messina, Contrada di Dio Sant'Agata, 98166 Messina, Italy; khaskhoussiamani105@gmail.com (A.K.); eproverbio@unime.it (E.P.)
2 National Interuniversity Consortium of Materials Science and Technology, INSTM, Via Giuseppe Giusti 9, 50121 Firenze, Italy
3 Department of Mathematics and Computer Science, Physical Sciences and Earth Sciences, University of Messina, Viale F.S. D'Alcontres n. 31, 98166 Messina, Italy; patanes@unime.it
* Correspondence: lcalabrese@unime.it; Tel.: +39-090-6765544

Received: 30 April 2019; Accepted: 27 May 2019; Published: 29 May 2019

Abstract: Superhydrophobicity is one of the most required surface properties for a wide range of application such as self-cleaning, anti-corrosion, oil-water separation, anti-icing, and anti-bioadhesion. Recently, several methods have been developed to produce nature inspired super-hydrophobic surfaces. Nevertheless, these methods require a complicated process and expensive equipment. In order to overcome these issues, we propose three different methods to obtain nature-inspired super-hydrophobic surfaces: short-term treatment with boiling water, HF/HCl and HNO_3/HCl concentrated solution etching. Afterwards, a thin layer of octadecylsilane was applied by in situ polymerization on all pre-treated surfaces. Eventually, all substrates were dried for 3 h at 100 °C to complete the silane curing. Scanning electron microscopy (SEM), contact angle measuring system and atomic force microscope (AFM) were used to characterize the surfaces. Surface morphology analysis showed that each method results in a specific dual hierarchical nano-/micro-structure. The corresponding water contact angles ranged from 160° to nearly 180°. The best results were observed for HF etched Al 6082 surface were water contact angle above 175° was achieved. Furthermore, a scheme able to assess the relationship between hydrophobic behavior and surface morphology was finally proposed.

Keywords: superhydrophobic; aluminum alloy; coating; silane; surface treatment

1. Introduction

Aluminum alloys are widely used in various industrial sectors thanks to the combination of properties such as: low density, high specific strength, and low cost. Such alloys are usually particularly susceptible to corrosion, and their low durability in aggressive environments is a limiting factor in industrial applications. However, by increasing the hydrophobic character of the metal surfaces a reduction of the interaction of the substrate with corrosive media or an enhancement of self-cleaning capabilities could be obtained. Therefore, obtaining a super-hydrophobic aluminum surfaces can be a suitable and potential effective solution to overcome the functional issues caused by corrosion or environmental contaminants [1–3].

In the last years, nature inspired super-hydrophobic surfaces acquired a large interest due to their potential and promising use for self cleaning, anti-icing, and corrosion resistance applications [4–6]. Super-hydrophobic aluminum surfaces can be a suitable and effective solution. Inspired by nature surfaces, such as lotus leaves, new functional surfaces with super-hydrophobic capabilities can be obtained combining hierarchical rough surface morphology with low surface energy materials [7–9].

Furthermore, in order to give an effective and reliable super hydrophobic behavior the coating surface must be characterized by low dynamic wettability hysteresis and low substrate tilt angle [10].

In this context, to understand the relationship among roughness texture, surface energy and hydrophobic behavior has received a relevant interest in order to promote the evolution of bio-mimetic super-hydrophobic surfaces. An effective parameter, re-entrant surface curvature, was identified to the design and optimization of super-hydrophobic and super-oleophobic substrate synergistically coupled with surface energy and roughness profile [11]. This information coupled with a specifically tailored textured surface plays a relevant role to design low energy superhydrophobic surfaces [12,13].

Several approaches, aimed to obtain super hydrophobic surfaces on aluminum alloy substrates have been proposed [14,15]. However, their implementation on an industrial level has been difficult due to their limited mechanical stability or relatively high processing times and costs [6]. In addition, many synthesis methods use fluorinated compounds that are harmful to human health and to the environment [16,17]. Consequently, the identification of synthesis techniques leading to super-hydrophobic surfaces by easy to use, cost-effective, and environmentally friendly approaches are particularly desired.

Chen et al. [18] observed that the chemical etching time has a relevant effect on the hydrophobic properties of an aluminum surface. Ruan et al. [19] studied various techniques of chemical etching and surface hydrophobizing methods, highlighting that an appropriate selection of process parameters has a fundamental effect on surface properties and therefore on hydrophobic or super-hydrophobic behavior of the surface itself.

Guo et al. [20] produced a superhydrophobic aluminum surface using a two-steps method. First, the aluminum substrate was treated on a zinc salt aqueous solution bath. Afterward a treatment with stearic acid was applied. The wettability of the aluminum surface changed from hydrophilic to superhydrophobic. In their approach, similarly to lotus leaf, a combined micro- and nano-scale rough structure was obtained indicating that the complex hierarchical surface morphology coupled to a low surface energy compound was responsible for high surface superhydrophobicity.

Analogously, Shi et al. [21] proposed a facile method to obtain a superhydrophobic surface on aluminum substrate by creating a hierarchical micro-flower structure based on a hydrothermal synthesis process, followed by lauric acid treatment to reduce the surface free energy.

Although significant efforts and research improvements have been made, further knowledge on easy and time-saving manufacturing methods of super-hydrophobic surfaces is required mainly in order to better relate the relationship between hierarchical structure and super-hydrophobic properties [22,23].

In the present paper, a super-hydrophobic surface with micro- and nano-roughness morphology was obtained on a 6082-T6 aluminum substrate by using three different surface pre-treatment procedures to create hierarchical rough structure: (i) boiling water treatment, (ii) wet chemical etching in HNO_3/HCl solution (volume ratio 1:3), and i(ii) wet chemical etching in HCl and HF solution. In order to exalt hydrophobic performances, a thin layer of octadecylsilane was applied by in situ polymerization on all pre-treated surfaces.

The effect of aluminum surface treatment on wettability and morphology of the aluminum substrate surface was assessed. The micro and nano rough structure of aluminum surfaces was evaluated combining scanning electron microscope and atomic force microscope observations. The super-hydrophobic behavior was assessed by performing WCA measurements by sessile drop tests. The results showed that all surface treatments stimulated the formation of a rough and hierarchical morphology with very large water contact angles. The best results were observed for HF etched Al 6082 surface were water contact angle (WCA) above 175° was achieved. A correlation between hydrophobic behavior and surface morphology was finally indicated.

2. Materials and Methods

2.1. Materials

Metal substrates were used with dimension 30 mm × 24 mm × 2 mm obtained from 1000 × 1000 × 2 laminated plate of commercially available EN AW-6082 T6 aluminum alloy, most commonly used for machining, offshore, or transport applications (chemical composition Si 0.70–1.3%; Mg 0.60–1.2%; Fe ≤ 0.50%; Cu ≤ 0.10%; Mn 0.40–1.0%; Cr ≤ 0.25%; Zn ≤ 0.20%; Ti ≤ 0.10%; Al balance). The mechanical properties of the alloy are reported in Table 1. Hydrochloric acid (37% concentration) and Nitric acid (60% concentration) were acquired from Carlo Erba. Hydrofluoric acid (48% concentration) and Octadecyltrimethoxysilane ($C_{21}H_{46}O_3Si$, 90%) were purchased from Sigma-Aldrich, St. Louis, MO, USA. Ultrapure bidistilled water was purchased from Best-Chemical, Vairono Patenora, Italy.

Table 1. 6082-T6 aluminum alloy chemical composition and main mechanical properties.

Ultimate Tensile Strength	Yield Tensile Strength	Elongation to Break
290 MPa	250 MPa	10%

2.2. Surface Treatment

All aluminum substrates were cleaned according to following procedure: ultrasonic cleaning in ethanol, acetone and ultra-pure water, and finally drying at room temperature in a silica-gel dryer.

In order to create hierarchical rough structure on as received surfaces, three different surface pre-treatment procedures were applied: (i) treatment in boiling water, (ii) HNO_3/HCl chemical etching, and (iii) HF/HCl chemical etching. In particular:

- Boiling H_2O: aluminum substrates were treated in ultrapure boiling water for 5 min and dried at 70° for 60 min.
- HNO_3/HCl: the cleaned samples were immersed in a mixture of HNO_3 and HCl (volume ratio 1:3) in ultra-pure water solution for 1 h.
- HF/HCl: a mixture acid solution was prepared by adding 73% by volume of HCl and 5% HF in ultra-pure water (22%). The aluminum substrates were immersed in this solution for 15 s.

Afterward, the etched samples were washed and cleaned in an ultrasonic bath with ultra-pure water to remove residuals acids and dried at 70° for 60 min. The resulting aluminum substrates were immersed in 0.1% by weight solution of Octadecyltrimethoxysilane (S18) in toluene for 10 min. Eventually, all substrates were dried for 3 h at 100 °C to complete the silane curing. In Table 2 the sample details realized for the research activity are summarized.

Table 2. Sample details.

Code	Surface Treatment	Silane
As received	–	–
AR-S	–	S18
A-F	HF/HCl solution	–
A-FS	HF/HCl solution	S18
A-N	HNO_3/HCl solution	–
A-NS	HNO_3/HCl solution	S18
A-W	Boiling water	–
A-WS	Boiling water	S18

2.3. Wettability Measurements

The static water contact angles of the coatings were measured using an Attension Theta Tensiometer (Attension, Biolin Scientific, Gothenburg, Sweden) equipment by Biolin Scientific according to the

sessile drop technique. A 3 µL distilled water droplet was set on the sample surface at room temperature (25 °C). A micro CCD camera (Attension, Biolin Scientific) on site equipped recorded the images of the droplets to be further analyzed using a suitable PC Attension software (OneAttension V. 2.3) to obtain the static contact angles of droplets on each of the coatings. Fifty replicas of water contact angle (WCA), located on the surface to obtain a regular grid, for each sample were performed.

2.4. Morphology Analysis

Morphological analysis of the surface features was carried out using a focused ion dual beam/scanning electron microscope (FIB-SEM ZEISS Crossbeam 540, ZEISS, Obwerkochen, Germany).

Roughness details of the surfaces were acquired by performing AFM maps obtained by an Explorer microscope (Veeco Instruments, Munich, Germany) equipped with a non-conductive silicon nitride probe model MSCT-EXMT-BF1 and working in contact mode.

All AFM measurements were performed in a controlled environmental chamber at temperature of 20 °C and a relative humidity of 60%. The scan rate was 0.2 Hz. The used tip had a radius of about 5 nm, the 50 µm × 50 µm scan area was sampled with 256 point/row, then the best resolution (distance between two points) was about 200 nm. The 5 µm × 5 µm scans had a resolution of about 20 nm. The RMS roughness for each group of samples was calculated as an average value of the measurements carried out over 3 areas on each sample using 3 samples in each group. All the images were post processed with plane and lines removal procedures and analyzed using Gwyddion 2.5 AFM software.

3. Results and Discussion

3.1. Morphological Analysis

Figure 1 shows the surface morphology of all treated surfaces samples. In the squared corner a high magnification of the surface morphology is reported.

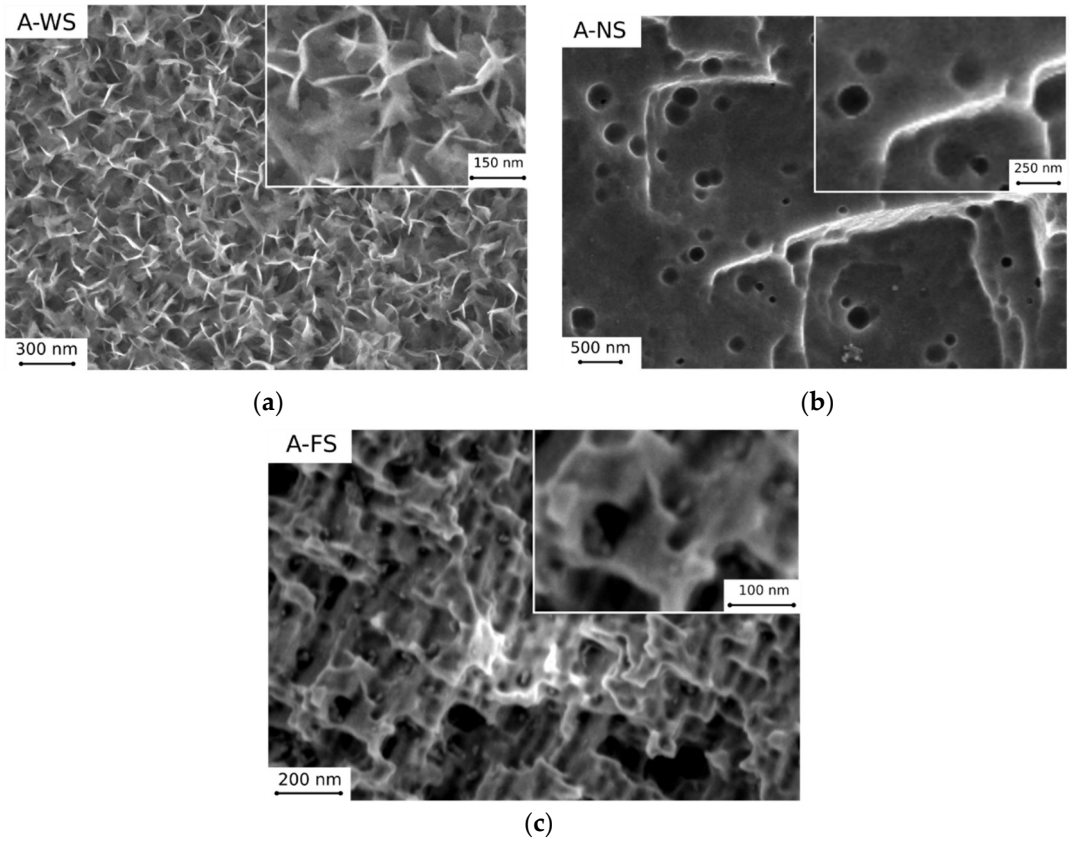

Figure 1. SEM micro-graphs of (**a**) A-WS; (**b**) A-NS, and (**c**) A-FS samples.

All etched samples showed significant surface modification induced by the pretreatment. The micrographies (Figure 1a–c) showed that all surfaces had a homogeneous structure. The thin silane layer did not influence surface microstructure. For sack of brevity images of un-silanized surfaces were not reported here (in the supporting information section, SEM image of as received surface (Figure S1), SEM image of A-W, A-F, and A-N samples (Figure S2); Photo of as received and after surface treatment aluminum alloy samples (Figure S3) are reported). No evidence of heterogeneity—due to a inefficient or localized surface attack during the pre-treatment process—was identified on the whole exposed surface of the sample. Analyzing the images, more useful information about hierarchical structure generated after all surface pre-treatment can be argued. Depending on the applied etching process different surface morphology features can be distinguished. In particular:

- Boiling H_2O: the surfaces appeared as a 3D flower-like structure. In fact, many 3D randomly oriented flakes clusters grew on the substrate. These flower-like clusters consisted of numerous petal-like flakes with a thickness of 30 nm. These neighboring platelets overlapped and connected with each other, thus generating a complex micro- and nano-scale upper-structure during growth. This result is a consequence of the formation of a protective surface film composed mainly by an amorphous or pseudo-amorphous boehmite with approximate $AlO(OH)\cdot H_2O$ [24–26]. The boehmite formation method is called boehmitage, and it is used in the industrial field as a surface engineering process in order to improve hydrophobicity and corrosion resistance of aluminum alloys [27].
- HNO_3/HCl: the surfaces obtained after nitric and chloridric acid diluted solution had a bimodal structure characterized by step like structure, at micro-scale level, and by regular small pits at nano-scale level. This two-level surface morphology significantly increased the effective surface area and the roughness surface profile. The smooth platelets had a length in the range 2–4 μm. The pits (diameter about 150 nm) were randomly distributed on the apparently smooth and planar areas of the platelets. This microstructure is a consequence of aluminum grain orientation, preferred dissolution planes and secondary phases distribution. The AA6082 alloy is indeed characterized by Fe–Mn inclusions with dimensions in the range 5–8 μm, randomly distribute in the whole surface [28]. Furthermore, several dislocations and defects are presents in the aluminum alloy matrix. These defects were more sensitive to the acidic etching solution than other locations of the metal substrate [29].
- HF/HCl: a bimodal structure was observed on the surface of treated aluminum. A main micro-structure was like a coral network structure with the presence of large deeper corrosion attack zones, while the nano-structure was similar to a pixel like structure with clear edges and corners. Only on this surface was a thin silane film observed on SEM images. The presence of the octadecylsilane film was mainly evidenced on the profile asperities. In fact, "pixel" corners, which were covered by the polymer monolayer, looked less acute still preserving the original shape.

In order to better analyze the coatings' surface morphology, AFM scanning was performed an all samples. Figure 2 compares 2D AFM maps (5 μm × 5 μm) for three types of surfaces. The visual AFM 2D images were morphologically compatible with SEM images placed next to it, for comparison. Figure 2a identifies the surface profile for A-WS sample. The roughness profile was due to "spheroidal" shaped vertex peaks covering the whole surface. This structure morphology can be related to the flower-like colonies of boehmite flakes, with a very small dimension, that grew during the boiling water treatment. As identifiable by the AFM profile for a reference line, the peaks and valleys of the A-WS profile were not very deep (a full gap between them is near to 200 nm), and the root width of each flower-like colony was very small (~60 nm). This implies a high number of similar peaks very close to each other. Therefore, the gate of the valley is only few nanometers. This could represent an obstacle for the homogeneous deposition on the whole profile of the S18 silane coating.

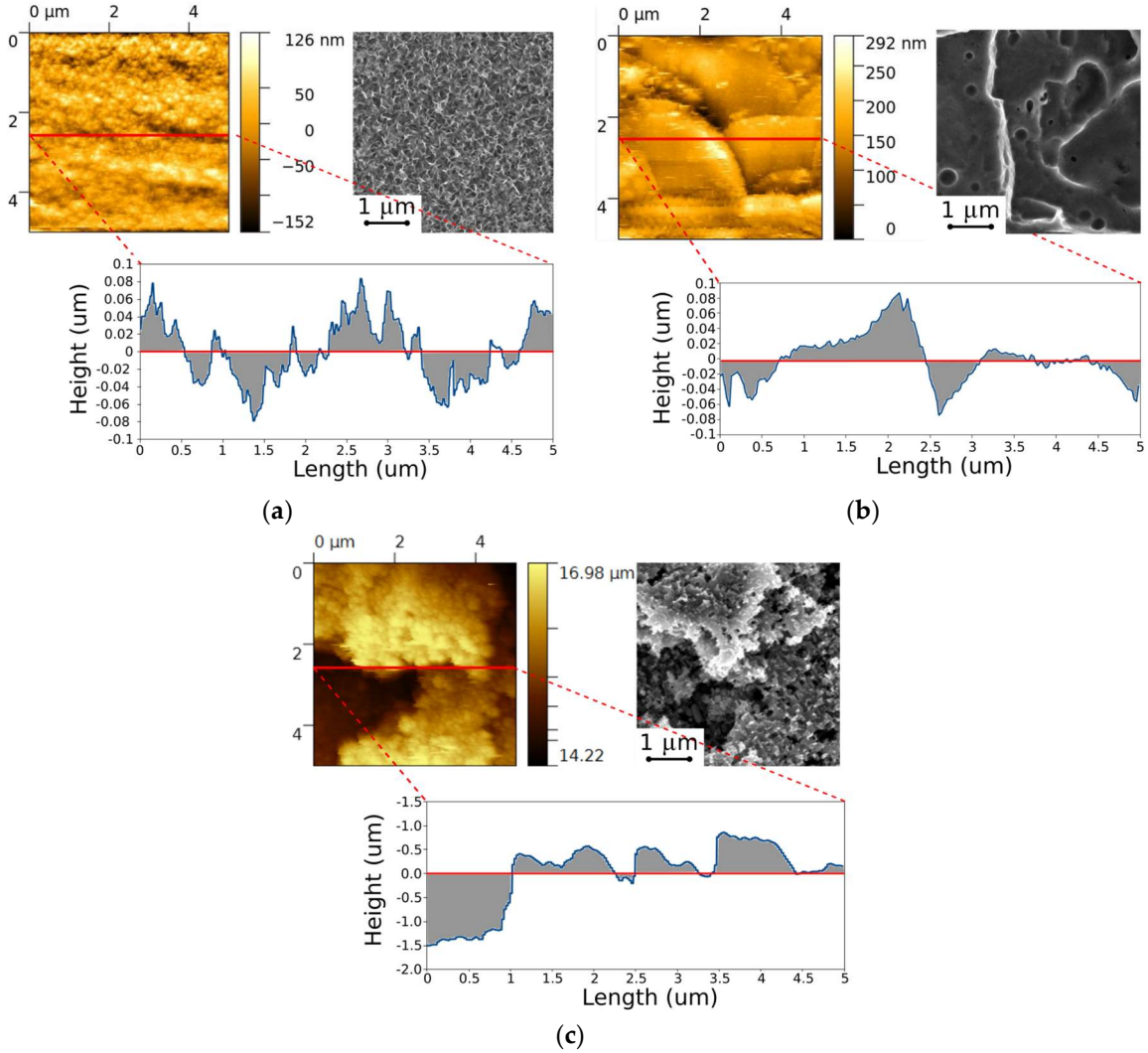

Figure 2. 2D AFM map of (**a**) A-WS; (**b**) A-NS, and (**c**) A-FS samples.

The surface morphology observed in Figure 2b, related to A-NS sample, is constituted by some platelets at micro level and some linear asperities located at a nan-oscale level. Furthermore, in the middle of the image, two wide cavities (diameter ~800–1000 nm), probably due to surface pits, can be identified. The structure although evidently rough, can be identified as a jagged plateau with steps. A reference line profile clearly showed the step transition (with depth of about 170 nm) between the two platelets.

Finally, Figure 2c shows the surface profile of the A-FS sample. The structure is well defined and several pixel-like blocks can be distinguished. A high roughness profile can be visually identified, indicating a deep and selective etching action of HF/HCl solution. The root size of each individual peak to valley profile was about 600 nm. The AFM profile for a reference line evidenced the bimodal roughness. Some large and deep valleys and peaks were coupled to a wide dispersed nano-roughness on the main profile, due to the pixeled sub-structure of AA6082 substrate after etching.

Based on the acquired data, statistical analysis of the roughness profile was performed to quantitatively compare the three surfaces. Table 3 summarizes the surface roughness parameters of the surfaces before and after silanization treatment. For brevity's sake, AFM 2D maps of the A-W, A-S, and A-F samples were not reported. 2D AFM maps (Figure S4) and a reference roughness profile (Figure S5) of the As-received aluminum alloys sample can be found in the supporting information Section.

Table 3. Roughness parameters determined by AFM image analysis.

Code	*R*a [nm]	*R*q [nm]	*R*sk	*R*ku	*R*SA [μm^2]
As-received	11.26	15.55	0.11	3.49	26.87
A-F	172.0	225.8	1.22	1.98	52.33
A-FS	136.5	171.5	-0.57	0.195	41.37
A-N	30.37	40.39	0.076	0.767	28.92
A-NS	15.12	20.40	0.046	2.11	27.85
A-W	29.48	39.28	0.177	1.397	31.94
A-WS	28.22	35.39	-0.121	0.057	30.46

*R*a is the arithmetic average height parameter and is the most common roughness parameter, defined as an absolute value, the difference in height of the asperities compared to the arithmetical mean of the surface. *R*q, the root mean square roughness, is defined as the standard deviation of the distribution of the surface heights. Despite *R*a, the *R*q parameter is more sensitive to profile peaks and valleys variations. The skewness, *R*sk, indicates the degree of bias of the roughness shape (asperity) and its value is related the degree of asymmetry of a surface profile. *R*sk = 0 if the distribution is symmetrical with as many peaks as valleys. *R*sk < 0 indicates that the height distribution is skewed above the mean plane and it is related to a profile with deep valleys. Conversely, a positive skewness parameter, height distribution skewed below the mean plane, is related to a profile characterized mainly with peaks and asperities. Finally, kurtosis, *R*ku, measures the sharpness of the roughness profile and its value is related to the degree of peakedness of a surface height distribution. This parameter is also sensitive to isolated peaks and valleys. *R*ku < 3 indicates height distribution skewed above the mean plane. *R*ku > 3 is related to spiked height distribution. When the kurtosis parameter is equal to 3, this indicates that the heights are characterized by a normal distribution (sharp and indented portions co-exist). Figure 3 shows a schematic representations of these two types of parameters (*R*ku and *R*sk). Finally, the RSA index indicates the real surface area determined using the surface AFM profile. It needs to be compared to the apparent surface area that is 25 μm^2.

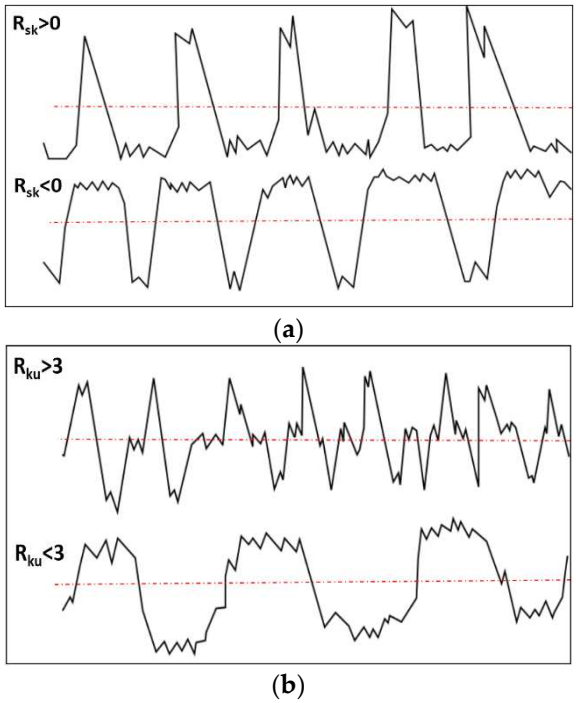

Figure 3. Representation of the Skewness parameter (**a**) and Kurtosis parameter (**b**).

Table 3 shows that the as received sample has a very low roughness (*R*a = 11.26 nm and *R*q = 15.55 nm). In addition, *R*sk ≈ 0 and *R*ku ≈ 3 parameters indicate that the height distribution was symmetric and MesoKurtic, hence the distribution is a Gaussian.

It can be also noted that the roughness, *R*a, was relatively low in A-NS and A-WS samples, about 30 nm. Instead, the A-FS sample showed a surface roughness about four time higher than that of the other samples (136.5 nm). The effect of silane coating on the surface roughness parameters of the A-F samples is clearly observed. In fact, *R*a and *R*q decreased by about 25% when the etched sample was coated with S18. In addition the *R*sk reduced from 1.22 to −0.57 indicating a more planar surface with roved peaks and the *R*ku decreased from 1.98 to 0.195 confirming that the A-F rough surface become flatter after coating. This behavior was also observed in the A-N and A-W samples. Furthermore, the A-NS sample was characterized by slight positive *R*sk parameter indicating a positive asymmetric distribution. In addition, *R*ku < 3 indicates a surface characterized by relatively low valleys and few peaks. However, the Skewness parameters of A-FS and A-WS were negative pointing out a morphological surface with large quantity of deep surface valleys and the distribution is negative asymmetry. This result is confirmed by Kurtosis parameter (*R*ku < 3), which reveals that the distribution had a few peaks. On the other hand, the A-FS and A-WS samples had 0.195 and 0.057 *R*ku parameter, respectively. This implies that the A-FS and A-WS had a more pointed and jagged shape distribution than that of the normal distribution. Furthermore, analyzing the RSA, it is possible to evidence that all profiles have a very high real surface area, quite different from the theoretical one (equal to 25 μm^2). Figure 4 shows the Roughness factor, *R*, defined as the ratio of the real surface area to its projection onto the horizontal plane for all the superhydrophobic surfaces. This parameter is obviously >1. Very high *R* parameters are related to very rough surfaces.

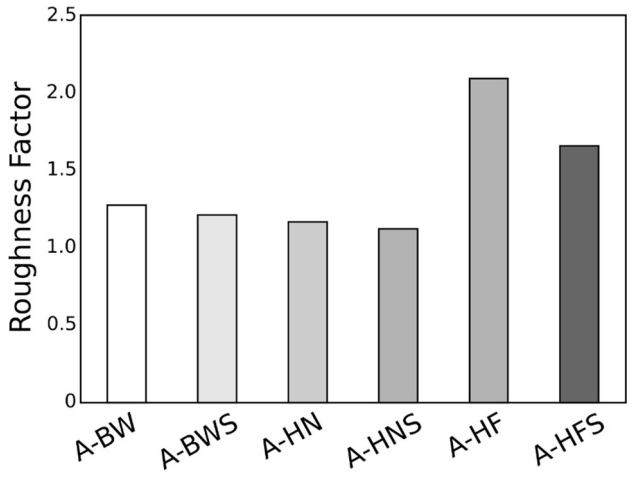

Figure 4. Roughness Factor for all surface treated samples.

The sample etched with HF/HCl solution evidenced a roughness parameter about 30% higher than other samples indicating that a very rough structure with high peaks and/or deep valleys was obtained. Instead, the HNO_3/HCl solution led to a surface profile of AA60682 alloy with a very low roughness factor (~1.12) indicating that the real surface area is only 12% larger than its projection on plane.

Analyzing the roughness parameters, *R*a and *R*q, for the A-N and A-F samples, a roughness reduction was observed after the octadecylsilane layer deposition. This behavior is attributable to the morphology surface profile of the samples. These samples were characterized by a bimodal micro- and nano-morphology. In particular, the macro morphology is constituted by wide rough jagged area homogeneously distributed on the whole surface. Some local asperities, due to selective attach of etching solution, occur at the micro-scale level (dimension in the range of 800–1100 nm). In this case, the octadecylsilane is probably able to reach on these cavities without mass diffusion limits. Therefore,

it is possible to hypothesize a good probability that silane molecules are able to bind in the grooves of these surfaces. This consideration is corroborated by the fact that the three reactive groups of the silane molecule prefer to react with three hydroxyl groups on the aluminum surface forming stable Si-O bonds. The broad jagged plateau in the profile could have a greater probability to have close hydroxyl groups. Instead, the peaks in the surface profile, due to a narrow and defined shape, should be less prone to interact with the silane molecules due to the reduced number of OH groups in such regions. Consequently, the silane molecules preferably bind to the surface hydroxyl groups located in the grooves and rough jagged zones, thus reducing the overall surface roughness as shown in Table 3.

Following silane deposition, a similar surface roughness in A-WS sample was observed compared to A-W. This behavior can be explained considering that, if the diffusion phenomenon limits or inhibits the silane molecule mass flow toward narrow cavities, a higher sensitivity of silane compound to grow up on extreme points of the etched surface could occurs, due to its chemical interaction with the metal substrate [30]. The A-W sample is constituted by peaks and valley with root dimension of about 15 nm, despite the A-NS and A-FS samples where asperities have dimension one order of magnitude larger (>400 nm). That led to a higher chemical reactivity on peak areas in A-W samples of the profile that on the valley one. Therefore, faster rates of silane layer formation can be obtained on surface extremities, and conversely a slower layer growth rate in the valleys. In these conditions, a S18 monolayer with a thickness almost near to a single molecule size is attended to form on the surface asperities of the substrates. That increases the peak height in the profile, partially compensating for the smoothing effect due to the valley saturation with S18 coatings [30].

3.2. Wettability Analysis

Figure 5 shows the wettability contour plot in distilled water for the A-NS (AA6082 substrate etched in HNO_3 + HCl acidic solution eventually coated with the octadecylsilane layer.

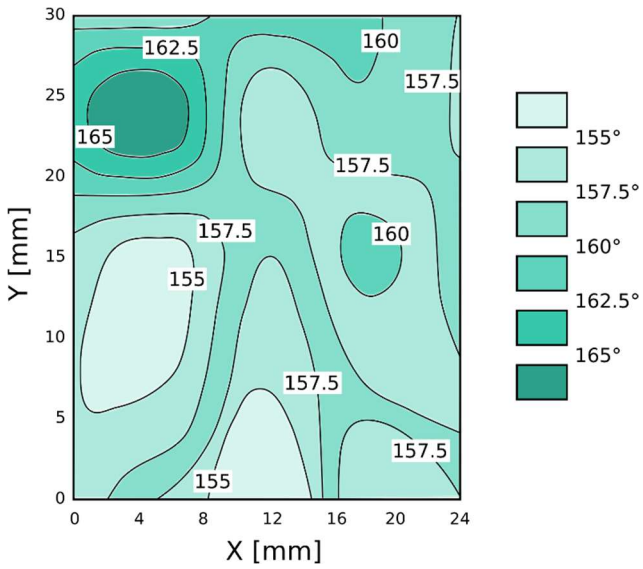

Figure 5. Wettability map of A-NS sample.

The graduated color bar identifies the contact angle value determined using a software digital image analysis. The contact angle value distribution was quite homogeneous. All the contact angle values were higher than 150°, indicating that the proposed surface treatment approach is suitable and effective for obtaining hierarchical structured super-hydrophobic surfaces. Although the presence of slightly localized not homogeneous areas can be also identified. In particular, a lower contact angle in the bottom side of the map than in the upper side can be identified. This contact angle trend can be ascribed with the difficulty to obtain almost stable coating deposition conditions by using dip-coating

procedure mainly in correspondence of surface discontinuity, such as silane solution meniscus or sample edges [31]. In particular, due to the dip coating process, a thickening of the silane layer may occur at the bottom edge of the specimen [32]. This entails the attenuation of the surface roughness due to the deposition of the silane layer on valley profile, inducing the local reduction of the water contact angle. Conversely, the upper edge, which is probably characterized by a more homogeneous layer of deposited silane, is characterized by higher water contact angle. This justifies the presence of highly localized low or high contact angle spots in these regions. In particular, by analyzing Figure 5, it is noted that the difference between the minimum and maximum contact angle found during the realization of the wettability map was about 10°. However, the average contact angle is 160.0°, with a standard deviation of 2.4°. Thus, the results achieved indicate a dispersion of the data, however, acceptable, with a suitable surface homogeneity considering also the extended analysis surface (720 mm^2). Similar considerations could be drawn by analyzing the wettability maps for the other specimens.

In order to better relate the hydrophobic behavior evolution to differing surface treatments on the aluminum support, Figure 6 shows the average contact angle values for all etched samples before and after silane layer deposition. For comparison, the water contact angle on as received sample (dotted red line) before and after silanization was also reported in Figure 6a,b, respectively. When the hydrophobicity increases, the contact angle of the droplets with the surface increases. Surfaces with contact angles lower than 90° are designated as hydrophilic. Surfaces that exhibit water contact angles above 150° are defined superhydrophobic.

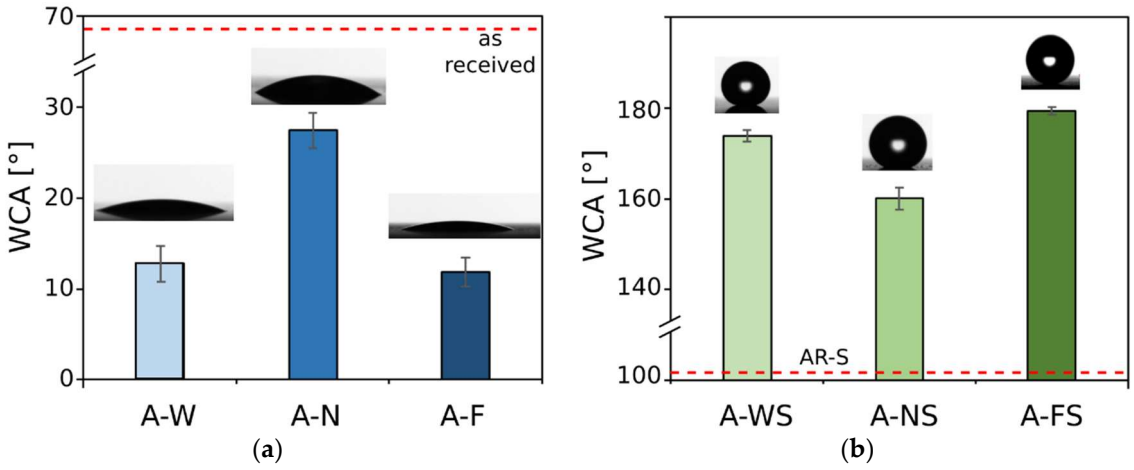

Figure 6. Contact angle for distilled water on surface treated and untreated aluminum alloy substrate (**a**) before silanization step and (**b**) after silanization dip-coating process. A dissimilar scale was used on vertical axes of the two plots to better highlight the differences between the several compared surfaces.

As observed in Table 2, related to AFM profile parameters, the surface roughness of etched samples (A-F, A-N, and A-W) was significantly higher than that of the received sample showing indeed a WCA of 68.7° ± 2.9°. Furthermore, their WCA was lower than bare aluminum surface and the roughness effect (Figure 6a). This behavior can be justified taking into account the hydrophilic nature of the aluminum surface. According to the Wenzel model, a roughness increase induces a decrease of the contact angle. Due to surface roughness treatment, the hydrophilic surface of aluminum apparently becomes more hydrophilic [33]. Therefore, it can be deduced that the surface morphology of un-silanized samples follow the Wenzel statement. The addition of a silane layer on the rough surface lead to a reduction of the surface energy thanks to the hydrophobic organic alkyd chains localized on the topside of the silane layer that significantly reduces the affinity of the surface with polar liquids [34]. As a consequence, all silanized surfaces evidenced a super-hydrophobic behavior (Figure 6b). The untreated AA6082 alloy sample after silanization showed contact angle in the order of 101° ± 2.1° (not reported here). Due to the coupled effect of surface silanization and micro-/nano-scale rough structure, a significant

improvement of super-hydrophobic behavior can be provided. In particular, the best results were observed for the A-FS sample, where average WCA of about 179° was observed. A-NS and A-WS samples showed average WCA of about 160° and 174°, respectively. These results are consistent with AFM measurements, where roughness profile observed on coated sample follows the order A-FS > A-WS > A-NS. This confirms that the deposition of a silane film on the aluminum substrate lead to the enhancement hydrophobic surface and to the increasing of the contact angle due to the presence of the S18 alkyl groups that shield the polar areas in the metal substrate.

Although all samples evidenced water contact angles above the threshold of 150°, only A-FS samples exhibited a low rolling angle (RA) < 5°. This implies that for this batch a transition from Wenzel to Cassie–Baxter regime could occur [35]. In this configuration, due to a high effective coupled action of high roughness and surface hydrophobicity, air pockets can remain entrapped on the profile, in correspondence on the droplet/substrate interface. That exalts the hydrophobic behavior of the surface, according to Cassie–Baxter model, leading to a very high contact angle [36]. Furthermore, the air entrapped in the water/solid interface reduces the interface contact area between the substrate and the liquid droplet allowing easier water rolling at low tilting angle.

This phenomenon cannot be ascribed on A-WS sample, where the rolling angle was higher than 90°. In this batch, also after a hydrophobic S18 layer addition, the surface regime was still in the Wenzel state. The Wenzel state is a contact mode in which the water droplet fully penetrates the surfaces grooves and the triple-phase liquid/air/solid contact line is stable and continuous. Thus, Wenzel's approach is called homogeneous wetting. According to the literature [37–39], the adhesion force was pointed out proportional to the van der Waals forces and the negative pressures produced by the air sealed in the surface. When the droplet was placed on the superhydrophobic surface, the negative pressures can be neglected. When the surface is turned, the surface air–water contact line changes from concave to convex so the volume of the sealed air increase. This sealed air expansion can increase the negative pressure, hence, liquid adhesion increases.

In Table 4, RA values for all samples are reported. The silanization-free samples do not show a tilt angle at which a rolling droplet occurred. A threshold value of 90° is indicated in the table. It is evident that only the A-FS samples showed a very effective tilting angle (<3°). Usually, the droplet starts to roll off just in planar position of the sample. Conversely, A-BS samples showed a tilt angle above 90°. A-NS samples evidenced a tilt angle of about 25°. Indicating an intermediate adhesion force of the droplet with the metal substrate.

Table 4. Rolling angle (RA) for silanized aluminum alloy surfaces.

Code	RA [°]
As-received	>90
AR-S	>90
A-F	>90
A-FS	<3
A-N	>90
A-NS	25 ± 5
A-W	>90
A-WS	>90

Therefore, the adhesion between surface and water droplets varies with the different roughening methods. The superhydrophobic surface with low adhesion, such as A-FS and A-NS where low rolling angle was observed, can be used for several industrial applications where self-cleaning or anti-corrosion performances are required [40,41]. While, the superhydrophobic surface with high adhesion, such as A-WS sample where no rolling angle was observed, can be used as a safe material for drug delivery in human body [42]. On the bio-inspired surfaces, the combination of conventional surface wettability theories (i.e., Cassie–Baxter and Wenzel models), is a suitable approach to determine superhydrophobic properties and to relate them with the hierarchical micro-/nano-structures of the

low-surface-energy substrate. Although when the wettability behavior is also involved with other liquids, the superoleophobic properties is a key factor and the re-entrant curvature topography becomes a valid surface tailoring approach [11].

3.3. Structural Surface Scheme of Super-Hydrophobic Coatings

Figure 7 shows the structural scheme of the superhydrophobic-coated surface of the AA6082 aluminum substrate. In the roughening step, a simplified presentation of the surface profile at varying surface treatment is reported.

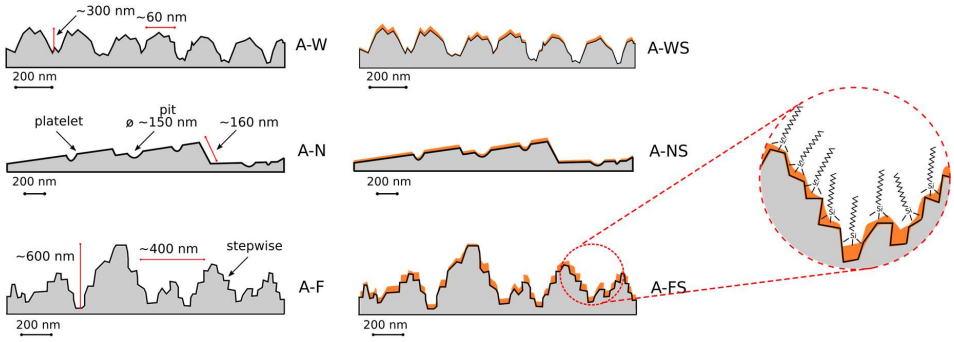

Figure 7. Scheme of structural super-hydrophobic surfaces of coatings.

A-W: (homogeneous nanometric roughness) the A-W sample is structured by well-defined and sharp peaks and valley. The cavities are about 300 nm deep. The surface is configured by several colonies of flakes randomly agglomerated with a flower-like structure. The distance among these clusters is variable and it is in the range of 60 nm and the topographic profile exhibits asperities at the nanometric scale.

A-N: (micrometric flatness; nanometric roughness) the structure of the A-N sample is very different. The HNO_3/HCl solution etching generated a plate like profile, with some platelets length of about 2–4 µm. The platelets follow different planes and steps of about 100–160 nm between platelets at different level can be schemed. Finally, small pits (diameter about 150 nm) are randomly located in the flatted area of platelets. Hence, the treatment with nitric and chloride acid solution involved the development of a slight jagged surface, at the micrometric scale, characterized by several steps at the platelet boundaries. These are coupled by a nanometric roughness induced by localized pitting attacks on the aluminum alloy.

A-F: (micrometric and nanometric roughness) for the A-F sample, according to the morphological analysis, a multi-level brick structure was proposed. It is characterized by higher cavity depth (~600 nm), each peak or valley root have a diameter of about 400 nm. The bimodel profile can be defined with micro-structures that identify the peaks and valleys of the profile and a very prominent nano-roughness in their walls (100 nm).

The silane dipping step allows to obtain the silane layer on the rough surface. The silicon atom in the octadecyl-silane can form three bonds with the aluminum surface thanks to the high reactivity of silanol groups (Si–OH) with the aluminum hydroxyl groups (Al–OH). This results in Al–O–Si bonds at the metal/silane interface. This interface helps to obtain a compact and adherent films with the substrate [43]. Instead, the functional long polymer chain of the silane compounds forms an organic surface monolayer, characterized by high hydrophobic properties. Thus, the obtained silane monolayer structure can have a preferential orientation of the hydrophobic alkyl chains, which enhance the hydrophobic performances of coating surfaces [44]. As reported in [45,46], the efficient hydrophobic behavior of the silane layer can be effectively designed using long alkyl chains molecules due to the regular and ordered arrangement, caused by the formation of long induced dipoles, that can acquire carbon chains that interact electrostatically with each other by van der Waals interactions. As a result,

alkyl silane self-assembled obtained monolayers can be obtained, exalting the hydrophobic properties of coatings.

The silane surface modification is not optimized when silanol groups interact with surface profiles of limited accessible sites. In this case, a more disordered silane layer can be obtained, inducing a lower contact angle with water [47]. Therefore the surface morphology plays a relevant role in the effective tailoring of surface hydrophobicity by silanization.

In particular, in the sample with only nanometric roughness (A-W sample), the silane coating can be deposited mainly in the peaks and in sporadic large cavities. This exalts the surface asperities and results in surfaces with efficient super-hydrophobic behavior. The sample A-N, characterized by a flat-wise structure, is homogeneously covered by the silane. The homogeneity can be hypothesized indirectly analyzing contact angle measurement maps (Figure 5) where a regular quite stable distribution of WCA is observed. Hence, surface roughness is significantly reduced, limiting the contribution of the hierarchical structure in the super-hydrophobic behavior of silanization. For a profile with micro- and nano-roughness, as in the A-F sample, an effective synergistic effect of bio-inspired rough surface and compact and homogeneous silane layer can be obtained, leading to very high WCA.

These results indicate that the hydrophilic or hydrophobic behavior of the aluminum surface can be designed by applying a specific etching treatment by tailoring the roughness profile coupled if required with a chemical modification in order to reduce surface energy. These results are promising for further development and investigation to better evaluate how the hierarchical morphology influences the interaction with liquids. Further studies aimed at exploiting WCA properties in static and dynamic conditions and the wettability capabilities with liquids at different polarities can represent an effective approach to providing further details on this issue.

4. Conclusions

Superhydrophobic surfaces on aluminum alloys were successfully obtained by three simple and cost-effective approaches. A two-step procedure was applied: (i) short term treatment with boiling water, HF/HCl and HNO_3/HCl concentrated solution etching, and (ii) an in situ polymerization method through octadecylsilane coupling agent applied on all pre-treated surfaces. Superhydrophobic aluminum surfaces were characterized by SEM, AFM, and contact angle measurement.

The effect of different roughness parameters and surface morphologies on the wettability of the samples were analyzed in details. Water boiling, HF/HCl, and HNO_3/HCl treatments offered very different structures. The surface morphology of all three approaches is structured by a peculiar dual hierarchical nano-/micro-roughness profile. The corresponding water contact angles ranged from 160° to nearly 180°. High water contact angle, above 175°, was observed for HF etched Al 6082 silanized surface. Furthermore, a scheme able to assess the relationship between hydrophobic behavior and surface morphology was finally proposed.

Supplementary Materials: The following are available online at http://www.mdpi.com/2079-6412/9/6/352/s1, Figure S1: SEM image of as received surface; Figure S2: SEM image of (a) A-W, (b) A-F, and (c) A-N samples; Figure S3: Photo of as received and after surface treatment aluminum alloy samples; Figure S4: 2D AFM image of as received surface; Figure S5: Reference roughness profile of as received surface.

Author Contributions: Conceptualization, L.C. and E.P.; Methodology, L.C.; Software, S.P.; Validation, E.P.; Formal Analysis, A.K. and S.P.; Investigation, A.K.; Data Curation, A.K. and L.C.; Writing—Original Draft Preparation, L.C.; Writing—Review and Editing, L.C. and E.P.; Supervision, E.P.;

Funding: This research received no external funding.

Conflicts of Interest: The authors declare no conflict of interest.

References

1. Mohamed, A.M.A.; Abdullah, A.M.; Younan, N.A. Corrosion behavior of superhydrophobic surfaces: A review. *Arab. J. Chem.* **2015**, *8*, 749–765. [CrossRef]

2. Jeevahan, J.; Chandrasekaran, M.; Joseph, G.B.; Durairaj, R.B.; Mageshwaran, G. Superhydrophobic surfaces: A review on fundamentals, applications, and challenges. *J. Coat. Technol. Res.* **2018**, *15*, 231–250. [CrossRef]
3. Cui, M.; Shen, Y.; Tian, H.; Yang, Y.; Feng, H.; Li, J. Influence of water adhesion of superhydrophobic surfaces on their anti-corrosive behavior. *Surf. Coat. Technol.* **2018**, *347*, 38–45. [CrossRef]
4. Lai, D.-L.; Kong, G.; Li, X.-C.; Che, C.-S. Corrosion resistance of ZnO nanorod superhydrophobic coatings with rose petal effect or lotus leaf effect. *J. Nanosci. Nanotechnol.* **2019**, *19*, 3919–3928. [CrossRef] [PubMed]
5. Nishimoto, S.; Bhushan, B. Bioinspired self-cleaning surfaces with superhydrophobicity, superoleophobicity, and superhydrophilicity. *RSC Adv.* **2013**, *3*, 671–690. [CrossRef]
6. Lin, Y.; Chen, H.; Wang, G.; Liu, A.; Lin, Y.; Chen, H.; Wang, G.; Liu, A. Recent progress in preparation and anti-icing applications of superhydrophobic coatings. *Coatings* **2018**, *8*, 208. [CrossRef]
7. Liu, Y.; Liu, J.; Li, S.; Han, Z.; Yu, S.; Ren, L. Fabrication of biomimetic super-hydrophobic surface on aluminum alloy. *J. Mater. Sci.* **2014**, *49*, 1624–1629. [CrossRef]
8. Zhao, Q.; Tang, T.; Wang, F. Fabrication of Superhydrophobic AA5052 aluminum alloy surface with improved corrosion resistance and self cleaning property. *Coatings* **2018**, *8*, 390. [CrossRef]
9. Zhang, D.; Li, L.; Wu, Y.; Zhu, B.; Song, H. One-step method for fabrication of bioinspired hierarchical superhydrophobic surface with robust stability. *Appl. Surf. Sci.* **2019**, *473*, 493–499. [CrossRef]
10. Urata, C.; Masheder, B.; Cheng, D.F.; Miranda, D.F.; Dunderdale, G.J.; Miyamae, T.; Hozumi, A. Why can organic liquids move easily on smooth alkyl-terminated surfaces? *Langmuir* **2014**, *30*, 4049–4055. [CrossRef] [PubMed]
11. Chen, L.; Guo, Z.; Liub, W. Outmatching superhydrophobicity: Bio-inspired re-entrant curvature for mighty superamphiphobicity in air. *Mater. Chem. A* **2017**, *5*, 14480–14507. [CrossRef]
12. Kadlečková, M.; Minařík, A.; Smolka, P.; Mráček, A.; Wrzecionko, E.; Novák, L.; Musilová, L.; Gajdošík, R. Preparation of textured surfaces on aluminum-alloy substrates. *Materials* **2018**, *12*, 109. [CrossRef]
13. Minařík, M.; Wrzecionko, E.; Minařík, A.; Grulich, O.; Smolka, P.; Musilová, L.; Junkar, I.; Primc, G.; Ptošková, B.; Mozetič, M. Preparation of hierarchically structured polystyrene surfaces with superhydrophobic properties by plasma-assisted fluorination. *Coatings* **2019**, *9*, 201. [CrossRef]
14. Zhang, D.; Wang, L.; Qian, H.; Li, X. Superhydrophobic surfaces for corrosion protection: A review of recent progresses and future directions. *J. Coat. Technol. Res.* **2016**, *13*, 11–29. [CrossRef]
15. Ran, M.; Zheng, W.; Wang, H. Fabrication of superhydrophobic surfaces for corrosion protection: A review. *Mater. Sci. Technol.* **2019**, *35*, 313–326. [CrossRef]
16. Vazirinasab, E.; Jafari, R.; Momen, G. Application of superhydrophobic coatings as a corrosion barrier: A review. *Surf. Coat. Technol.* **2018**, *341*, 40–56. [CrossRef]
17. Petr, M.; Hanuš, J.; Kylián, O.; Kratochvíl, J.; Solař, P.; Slavínská, D.; Biederman, H. Superhydrophobic fluorine-free hierarchical coatings produced by vacuum based method. *Mater. Lett.* **2016**, *167*, 30–33. [CrossRef]
18. Chen, Z.; Guo, Y.; Fang, S. A facial approach to fabricate superhydrophobic aluminum surface. *Surf. Interface Anal.* **2010**, *42*, 1–6. [CrossRef]
19. Ruan, M.; Li, W.; Wang, B.; Luo, Q.; Ma, F.; Yu, Z. Optimal conditions for the preparation of superhydrophobic surfaces on al substrates using a simple etching approach. *Appl. Surf. Sci.* **2012**, *258*, 7031–7035. [CrossRef]
20. Guo, Y.; Wang, Q.; Wang, T. Facile fabrication of superhydrophobic surface with micro/nanoscale binary structures on aluminum substrate. *Appl. Surf. Sci.* **2011**, *253*, 5831–5836. [CrossRef]
21. Shi, Y.; Xiao, X.; Zhang, W. Facile fabrication of superhydrophobic surface with needle-like microflower structure on aluminum substrate. *J. Coat. Technol. Res.* **2015**, *12*, 1143–1151. [CrossRef]
22. Chen, F.F.; Yang, Z.Y.; Zhu, Y.J.; Xiong, Z.C.; Dong, L.Y.; Lu, B.Q.; Wu, J.; Yang, R.L. Low-cost and scaled-up production of fluorine-free, substrate-independent, large-area superhydrophobic coatings based on hydroxyapatite nanowire bundles. *Chem. A Eur. J.* **2018**, *24*, 416–424. [CrossRef]
23. Simpson, J.T.; Hunter, S.R.; Aytug, T. Superhydrophobic materials and coatings: A review. *Rep. Prog. Phys.* **2015**, *78*, 086501. [CrossRef]
24. Geiculescu, A.C.; Strange, T.F. A microstructural investigation of low-temperature crystalline alumina films grown on aluminum. *Thin Solid Films* **2003**, *426*, 160–171. [CrossRef]
25. Underhill, P.R.; Rider, A.N. Hydrated oxide film growth on aluminium alloys immersed in warm water. *Surf. Coat. Technol.* **2005**, *192*, 199–207. [CrossRef]

26. Feng, L.; Yan, Z.; Qiang, X.; Liu, Y.; Wang, Y. Facile formation of superhydrophobic aluminum alloy surface and corrosion-resistant behavior. *Appl. Phys. A Mater. Sci. Process.* **2016**, *122*, 165. [CrossRef]
27. Jafari, R.; Farzaneh, M. Fabrication of superhydrophobic nanostructured surface on aluminum alloy. *Appl. Phys. A Mater. Sci. Process.* **2011**, *102*, 195–199. [CrossRef]
28. Calabrese, L.; Bruzzaniti, P.; Proverbio, E. Pitting corrosion of aluminum alloys in anhydrous ethanol. *Mater. Corros.* **2018**, *69*, 1815–1826. [CrossRef]
29. Zhang, Y.; Wu, J.; Yu, X.; Wu, H. Low-cost one-step fabrication of superhydrophobic surface on Al alloy. *Appl. Surf. Sci.* **2011**, *257*, 7928–7931. [CrossRef]
30. Rahimi, M.; Fojan, P.; Gurevich, L.; Afshari, A. Effects of aluminium surface morphology and chemical modification on wettability. *Appl. Surf. Sci.* **2014**, *296*, 124–132. [CrossRef]
31. Chen, M.M.; Zhang, X.M.; Ma, J.P.; Chen, S.C.; Chen, W.X.; Feng, L.F. Experimental study on film thickness and the problem of free surface film flow in dip coating. *Asia-Pac. J. Chem. Eng.* **2016**, *11*, 695–704. [CrossRef]
32. Calabrese, L.; Bonaccorsi, L.; Caprì, A.; Proverbio, E. Adhesion aspects of hydrophobic silane zeolite coatings for corrosion protection of aluminium substrate. *Prog. Org. Coat.* **2014**, *77*, 1341–1350. [CrossRef]
33. Possart, W.; Kamusewitz, H. Wetting and scanning force microscopy on rough polymer surfaces: Wenzel's roughness factor and the thermodynamic contact angle. *Appl. Phys. A Mater. Sci. Process.* **2003**, *76*, 899–902. [CrossRef]
34. Calabrese, L.; Bonaccorsi, L.; Caprì, A.; Proverbio, E. Electrochemical behavior of hydrophobic silane–zeolite coatings for corrosion protection of aluminum substrate. *J. Coat. Technol. Res.* **2014**, *11*, 883–898. [CrossRef]
35. Lafuma, A.; Quéré, D. Superhydrophobic states. *Nat. Mater.* **2003**, *2*, 457–460. [CrossRef]
36. Belaud, V.; Valette, S.; Stremsdoerfer, G.; Bigerelle, M.; Benayoun, S. Wettability versus roughness: Multi-scales approach. *Tribol. Int.* **2015**, *82*, 343–349. [CrossRef]
37. Xiang, T.; Zhang, M.; Li, C.; Zheng, S.; Ding, S.; Wang, J.; Dong, C.; Yang, L. A facile method for fabrication of superhydrophobic surface with controllable water adhesion and its applications. *J. Alloy. Compd.* **2017**, *704*, 170–179. [CrossRef]
38. Cheng, Z.; Du, M.; Lai, H.; Zhang, N.; Sun, K. From petal effect to lotus effect: A facile solution immersion process for the fabrication of super-hydrophobic surfaces with controlled adhesion. *Nanoscale* **2013**, *5*, 2776–2783. [CrossRef] [PubMed]
39. West, J.B. The original presentation of Boyle's law. *J. Appl. Physiol.* **1999**, *87*, 1543–1545. [CrossRef]
40. Zhang, B.; Zhu, Q.; Li, Y.; Hou, B. Facile fluorine-free one step fabrication of superhydrophobic aluminum surface towards self-cleaning and marine anticorrosion. *Chem. Eng. J.* **2018**, *352*, 625–633. [CrossRef]
41. Varshney, P.; Mohapatra, S.; Kumar, A. Fabrication of Mechanically Stable Superhydrophobic Aluminium Surface with Excellent Self-Cleaning and Anti-Fogging Properties. *Biomimetics* **2017**, *2*, 2. [CrossRef] [PubMed]
42. Yohe, S.T.; Herrera, V.L.M.; Colson, Y.L.; Grinstaff, M.W. 3D superhydrophobic electrospun meshes as reinforcement materials for sustained local delivery against colorecal cancer cells. *J. Control. Release* **2012**, *162*, 92–101. [CrossRef] [PubMed]
43. van Ooij, W.J.; Zhu, D.; Stacy, M.; Seth, A.; Mugada, T.; Gandhi, J.; Puomi, P. Corrosion protection properties of organofunctional silanes-An overview. *Tsinghua Sci. Technol.* **2005**, *10*, 639–664. [CrossRef]
44. Calabrese, L.; Bonaccorsi, L.; Caprì, A.; Proverbio, E. Effect of silane matrix composition on performances of zeolite composite coatings. *Prog. Org. Coat.* **2016**, *101*, 100–110. [CrossRef]
45. Kulinich, S.A.; Farzaneh, M. Alkylsilane self-assembled monolayers: Modeling their wetting characteristics. *Appl. Surf. Sci.* **2004**, *230*, 232–240. [CrossRef]
46. Calabrese, L.; Bonaccorsi, L.; Capri, A.; Proverbio, E. Effect of silane matrix on corrosion protection of zeolite based composite coatings. *Metall. Ital.* **2014**, *106*, 35–39.
47. Calabrese, L.; Bonaccorsi, L.; Proverbio, E. Corrosion protection of aluminum 6061 in NaCl solution by silane-zeolite composite coatings. *J. Coat. Technol. Res.* **2012**, *9*, 597–607. [CrossRef]